

# NOS-Gate: Queue-Aware Streaming IDS for Consumer Gateways under Timing-Controlled Evasion

Muhammad Bilal , Senior Member, IEEE, Omer Tariq  Hasan Ahmed

**Abstract**—Timing and burst patterns can leak through encryption, and an adaptive adversary can exploit them. This undermines metadata-only detection in a stand-alone consumer gateway. Therefore, consumer gateways need streaming intrusion detection on encrypted traffic using metadata only, under tight CPU and latency budgets. We present a streaming IDS for stand-alone gateways that instantiates a lightweight two-state unit derived from Network-Optimised Spiking (NOS) dynamics [1] per flow, named *NOS-Gate*. NOS-Gate scores fixed-length windows of metadata features and, under a  $K$ -of- $M$  persistence rule, triggers a reversible mitigation that temporarily reduces the flow’s weight under weighted fair queueing (WFQ). We evaluate NOS-Gate under timing-controlled evasion using an executable *worlds* benchmark that specifies benign device processes, auditable attacker budgets, contention structure, and packet-level WFQ replay to quantify queue impact. All methods are calibrated label-free via burn-in quantile thresholding. Across multiple reproducible worlds and malicious episodes, at an achieved 0.1% false-positive operating point, NOS-Gate attains 0.952 incident recall versus 0.857 for the best baseline in these runs. Under gating, it reduces p99.9 queueing delay and p99.9 collateral delay with a mean scoring cost of  $\approx 2.09 \mu\text{s}$  per flow-window on CPU.

**Index Terms**—consumer gateway, metadata-only intrusion detection, timing-controlled evasion, network-optimised spiking (NOS), weighted fair queueing

## I. INTRODUCTION

Home gateways and consumer hubs sit between consumer devices and encrypted services (web and cloud). Encryption limits payload inspection at the edge, but it does not remove traffic side channels such as timing, packet sizes, and burst structure [2], [3]. These signals have been used for device identification and security monitoring [4]–[7], but the gateway setting imposes two constraints that shape what is practical. First, detection must run continuously with low latency and modest CPU, which makes large models and heavy training difficult to justify [8], [9]. Second, an attacker can often change packet timing without changing endpoints, ports, or encrypted content.

Timing control is therefore a realistic evasion surface. Prior work shows that timing and burst patterns can still leak structure under encryption [3]. The same idea can be used offensively: an attacker can reshape inter-arrival times and bursts to resemble

Muhammad Bilal and Hasan Ahmed are with the School of Computing and Communications, Lancaster University, LA1 4WA, Lancaster, U.K. E-mail: m.bilal@ieee.org, h.ahmed@lancaster.ac.uk.

Omer Tariq is with the School of Computing, Korea Advanced Institute of Science and Technology, Daejeon, 34141, South Korea. E-mail: omertariq@kaist.ac.kr

benign device rhythms while still pursuing an hidden attack objective [10], [11]. This raises an operational IDS question that is not captured well by offline accuracy alone: can a gateway detect quickly enough to act, at a low false-alarm rate, using only metadata, against timing-shaped adversaries?

We address this question with *NOS-Gate*, a streaming IDS for stand-alone gateways derived from Network-Optimised Spiking (NOS) dynamics [1], [12]. NOS-Gate instantiates a lightweight two-state dynamical unit per flow. An excitability-like state accumulates evidence from normalised metadata deviations, while a recovery-like state provides short-term memory and suppresses repeated triggering. The detector emits an event-like surrogate and applies a persistence rule to stabilise decisions. This design is deliberately simple: compact state updates fit gateway budgets while still expressing persistence and hysteresis, which are hard to add to a simple window-based score with no memory. [13], [14].

Crucially, we connect detection to a gateway-safe action. When alarms persist, NOS-Gate temporarily reduces the weight of the flagged flow under weighted fair queueing (WFQ). This aims to reduce queue-tail harm while limiting collateral impact on benign traffic [15]–[18]. Figure 1 summarises the online loop (windowing, scoring, persistence, and WFQ gating) and the offline evaluation harness used to measure queue impact.

Recent encrypted-traffic security systems have improved robustness and deployment realism, but they usually make different assumptions than a consumer gateway IDS. HyperVision detects unknown encrypted malicious traffic using flow-interaction graphs [19]. RAPIER studies detection under low-quality training data [20]. Wedjat targets evasive behaviour using real-time causal analysis [21]. ET-SSL explores self-supervised contrastive learning for encrypted-traffic anomaly detection [22]. These works reinforce that encrypted side channels remain useful, but they typically do not evaluate the full gateway action loop (detection  $\rightarrow$  mitigation  $\rightarrow$  queue impact) under an explicit timing-control budget, and they do not standardise a stand-alone label-free calibration protocol. NOS-Gate is built around those gateway requirements.

A second contribution is evaluation methodology. Public IoT corpora and botnet traces are valuable, but they often provide limited coverage of timing-controlled evasion and rarely offer an auditable link from attacker constraints to queue-level harm at the gateway [23]–[25]. We therefore introduce an executable *worlds* benchmark that specifies benign device processes and contention structure, constrains adversaries by auditable budgets, and uses packet-level WFQ replay to quantify

user-visible impact. We evaluate all detectors under the same stand-alone, label-free protocol: an assumed-benign burn-in segment, per-flow thresholds set by high quantiles of burn-in scores, and labels used only for reporting on held-out time [8], [9], [26].

We make three contributions that together support a practical, auditable gateway IDS under timing-controlled evasion:

- We propose a two-state detector *NOS-Gate*, a streaming, metadata-only gateway IDS with a direct action hook: a per-flow two-state detector with persistence-based alerting that drives WFQ deprioritisation.
- We introduce a reproducible *worlds* benchmark with published contention structure, auditable attacker budgets, and packet-level WFQ replay, enabling queue-tail and collateral evaluation under timing-shaped attacks.
- We standardise a stand-alone operating protocol at explicit false-alarm budgets using burn-in quantile thresholding and persistence, and we report achieved false-positive rates, incident recall, and time-to-detect under the same calibration rule..

Under the published feature contract and attacker budgets, NOS-Gate provides a stronger detection-and-action trade-off than the evaluated label-free baselines: higher incident detection at the same achieved false-alarm budget, and improved queue-tail outcomes when WFQ gating is enabled. This work do not claim payload inspection, DPI deployment in ISP-grade firmware, or that synthetic worlds reproduce any single public dataset. We present the benchmark as a falsifiable protocol: new worlds, budgets, and contention structures can be added to test generality and failure modes. Table I groups representative encrypted-traffic systems by operating model and evaluation axes that matter for consumer gateway comparability.

## II. SYSTEM MODEL (CONSUMER GATEWAY)

We model a stand-alone consumer gateway that observes packet metadata behind NAT and produces streaming decisions at a fixed cadence. Time is divided into non-overlapping windows of length  $\Delta t = 250$  ms (Section III-A). The detector operates on directed five-tuple flows and is calibrated without labels using an assumed-benign burn-in segment. Flows may start and stop during a horizon. For a newly observed flow, we compute scores immediately, but we enable the per-flow quantile threshold only after the flow has accumulated enough burn-in windows to estimate a stable high quantile.

*Inputs and operating protocol.:* The feature stream is limited to fields visible at the gateway: packet headers, timestamps, and sizes, plus DNS and TLS handshake metadata when present (for example, SNI and certificate validity days). We do not use payload bytes, deep packet inspection features, or host logs. If DNS/TLS fields are absent, NOS-Gate falls back to timing and size features without changing the model. To avoid mixing feature dimensions within a run, we evaluate a fixed feature contract per run (for example, timing+contention only, or timing plus DNS/TLS when uniformly available). The run manifest records the feature contract used.

For each flow  $i$  and window  $t$ , the detector outputs a score  $s_{i,t}$  and an alarm  $a_{i,t} = \mathbb{I}\{s_{i,t} \geq \vartheta_i\}$ . Thresholds are calibrated

label-free from the burn-in segment. Let the horizon be  $H$  windows and let the burn-in length be  $H_{\text{burn}} = \lfloor 0.6H \rfloor$ . We set

$$\vartheta_i = \text{Quantile}_q\left(\{s_{i,t} : t = 0, \dots, H_{\text{burn}} - 1\}\right), \quad (1)$$

with  $q \in \{0.99, 0.999\}$  as the operating knob (we report both). Performance is reported on the remaining test segment using the same frozen  $\vartheta_i$ , including the achieved benign false-positive rate.

To avoid flapping, we apply a  $K$ -of- $M$  persistence rule. A flow becomes actionable only if at least  $K$  alarms occur in the most recent  $M$  windows (defaults  $K = 3$ ,  $M = 8$ ):

$$z_{i,t} = \mathbb{I}\left\{ \sum_{\tau=t-M+1}^t a_{i,\tau} \geq K \right\}, \quad (2)$$

where missing past windows at flow start contribute zero. We clear  $z_{i,t}$  only after  $M$  consecutive windows with  $a_{i,t} = 0$ , which yields a stable on/off action signal.

*Queueing model and WFQ action.:* We evaluate action impact through packet-level queue replay at the gateway. Flows that share the uplink enter a work-conserving weighted fair queueing (WFQ) scheduler. Let  $\omega_i(t)$  be the weight assigned to flow  $i$  at time  $t$ . Under normal operation,  $\omega_i(t) = \omega_0$ . Under gating, a flow that is actionable ( $z_{i,t} = 1$ ) is deprioritised by setting  $\omega_i(t) = \omega_-$  with  $\omega_- < \omega_0$  for a quarantine duration  $T_g$  (or until the flag clears, whichever is longer). We report both detection metrics and queue-tail metrics, including collateral delay experienced by benign flows. WFQ gating is reversible and avoids immediate blocking while still limiting queue-tail harm when alarms persist (Figure 1).

### A. *Worlds* benchmark: contract and outputs

The primary evidence in this paper is produced by a reproducible synthetic benchmark called *worlds*. A *world* is a fully specified, executable instance that fixes benign device processes, malicious episode generators, contention structure, and an evaluation harness for queue impact. Each world publishes: (i) benign device classes and traffic generators, (ii) malicious episode generators, (iii) contention structure (cliques and weights  $W$ , including a target band for  $\rho(W)$ ), (iv) a packet trace with flow keys, (v) the derived windowed feature stream, (vi) labels used only for reporting, and (vii) WFQ replay configuration and queue summaries. The released artefacts include world ids, random seeds, configuration hashes, and manifests linking raw and derived outputs.

*Budgets, feasibility, and timeline.:* Timing-controlled evasion is defined by auditable operational budgets  $(R_i^{\min}, \varepsilon, \delta_q)$  and a feasibility protocol. We define these budgets in the threat model (Section III-D, Table II) and report feasibility rates for each budget setting. Within each world, time is split chronologically into burn-in, validation, and test. During burn-in we update the online normaliser, train label-free baselines, and collect burn-in scores to set per-flow thresholds  $\vartheta_i$ . Validation is used only for design-time selection from a small fixed hyperparameter grid. Test uses frozen detectors and frozen  $\vartheta_i$  to report achieved false-positive rate, recall, detection delay, and queue-tail outcomes with and without gating.

TABLE I  
COMPARISON OF ENCRYPTED-TRAFFIC SECURITY SYSTEMS FOR STAND-ALONE GATEWAY DEPLOYMENT

Group / work	Inputs	Training & calibration	Online	Robustness / evasion	Action / impact	Fit to assumptions	NOS-Gate
<i>G0. Gateway action loop (detection → mitigation → queue impact)</i>							
NOS-Gate (this paper)	Per-flow metadata + contention signals	Label-free burn-in; per-flow high-quantile thresholds; $K$ -of- $M$ persistence	Yes	Explicit timing-control budgets; feasibility reported	WFQ weight gating; queue-tail & collateral via replay	Direct match: stand-alone calibration and action-impact loop	
<i>G1. Interaction-aware encrypted-traffic detection (detection-first)</i>							
HyperVision [19]	Encrypted traffic features + flow-interaction graph	Dataset-trained; calibration follows paper/dataset protocol	Yes	Targets unknown/novel threats (not posed as timing-budget shaping)	No mitigation or queue impact	Closest on online inference, but different calibration and threat model	
<i>G2. Robust learning under weak supervision / data quality shift</i>							
RAPIER [20]	Encrypted traffic detection features	Robust training under low-quality data; typically offline	Often	Robustness to data quality shift (rather than timing budgets)	No action loop	Useful robustness angle, but not an action-coupled gateway protocol	
<i>G3. Evasion emphasis (action-free evaluation)</i>							
Wedjat [21]	Encrypted traffic signals + causal analysis components	Dataset-driven learning and evaluation protocol	Yes	Explicit evasion emphasis; real-time impact framing	No mitigation or queue impact	Threat focus is closer, but lacks stand-alone calibration and impact loop	
<i>G4. Self-supervised representation learning (pretrain then downstream scoring)</i>							
ET-SSL [22]	Encrypted traffic features	Self-supervised pretraining; downstream calibration varies by use case	Often	Not formulated as timing-budget shaping; robustness depends on downstream task	No action loop	Promising feature learning, but comparability hinges on calibration and impact evaluation	

### III. THREAT MODEL

We consider a stand-alone consumer gateway that observes packet metadata behind NAT and emits streaming, flow-level decisions at a fixed window cadence. The attacker can reshape packet timing and, within bounds, packet sizes. Evasion is constrained by explicit operational budgets that make attacks auditable in our *worlds* benchmark.

#### A. Observation model and feature access

Packets are indexed by  $n$ , with arrival times  $t_n \in \mathbb{R}_{\geq 0}$  and lengths  $\ell_n \in [\ell_{\min}, \ell_{\max}]$ . A directed flow  $i$  is the five-tuple  $(\text{srcIP}, \text{dstIP}, \text{srcPort}, \text{dstPort}, \text{proto})$ . Time is partitioned into non-overlapping windows of length  $\Delta t$ , indexed by  $t \in \{0, 1, \dots, H - 1\}$ .

Let  $N_{i,t}$  be the number of packets from flow  $i$  in window  $t$ ,  

$$N_{i,t} = |\{n \in i : t_n \in [t\Delta t, (t+1)\Delta t]\}|. \quad (3)$$

When  $N_{i,t} \geq 2$ , define the inter-arrival-time (IAT) multiset within the window as

$$\mathcal{I}_{i,t} = \{t_{n+1} - t_n : n, n+1 \in i, t_n, t_{n+1} \in [t\Delta t, (t+1)\Delta t]\}. \quad (4)$$

The detector receives a feature vector  $x_{i,t} \in \mathbb{R}^d$  computed causally from packet timestamps and sizes, optional DNS/TLS handshake metadata when visible, and contention signals available at the gateway (Section V). No payload content and no host logs are used.

#### B. Benign traffic and malicious episodes

Within a world, each flow  $i$  is generated by either a benign process or a malicious episode generator. Let  $\mathbb{P}_i^{\text{ben}}$  and  $\mathbb{P}_i^{\text{mal}}$  denote the per-window distributions of  $x_{i,t}$  in benign and malicious modes. Flows that share the same uplink scheduling domain are grouped into contention cliques. We represent clique-level interference using a nonnegative weight matrix

$W = [w_{ij}]$ , and we report its spectral radius  $\rho(W)$  as a compact summary of contention intensity.

#### C. Adversary capabilities and knowledge

We assume a remote adversary that can compromise IoT devices and generate malicious traffic while remaining behind NAT. The adversary can: (i) use encrypted channels, (ii) choose protocols and endpoints consistent with common device behaviour, and (iii) reshape packet timing and, within bounds, packet sizes. The adversary knows the feature contract and the window length  $\Delta t$ .

The defender calibrates thresholds in a label-free, stand-alone way during an assumed-benign burn-in segment (Section II). This reflects a standard operational assumption: burn-in is not dominated by malicious behaviour.

#### D. Operational budgets for timing-controlled evasion

Evasion is constrained by three budgets that capture objective, timing stealth, and contention stealth. For a flow  $i$ , the budgets are  $(R_i^{\text{min}}, \varepsilon, \delta_q)$  and are enforced by the worlds generator (Table II).

For timing stealth, each malicious flow  $i$  is paired with a benign IAT reference distribution  $P_i^{\text{ben,iat}}$  constructed within the same world, using the benign process that matches  $i$ 's device class and endpoint template. This makes the timing constraint auditable per world.

IAT-based distortion is undefined when  $N_{i,t} < 2$ . We therefore apply the timing distortion constraint only on windows that contain at least two packets:

$$\mathcal{T}_i = \{t \in \{0, \dots, H - 1\} : N_{i,t} \geq 2\}. \quad (5)$$

This does not remove constraints in sparse windows. The detector still observes packet counts, rates, and size-based features in every window. The restriction applies only to the IAT distortion term because it is undefined otherwise.

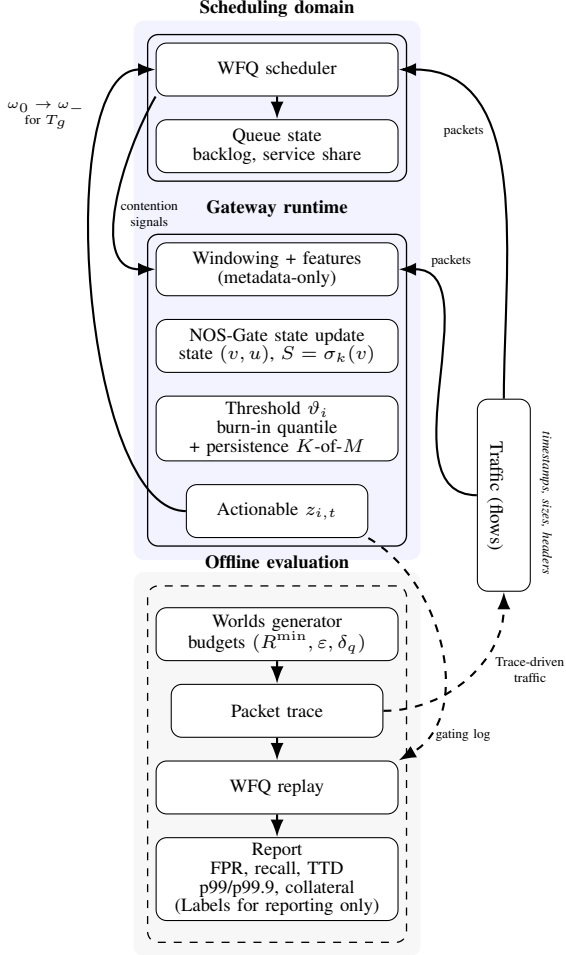


Fig. 1. Online, the gateway windows metadata-only traffic, updates NOS-Gate state  $(v, u)$ , applies burn-in quantile thresholding and a  $K$ -of- $M$  persistence rule to produce an actionable flag  $z_{i,t}$ , and temporarily reduces WFQ weight  $\omega_0 \rightarrow \omega_-$  for  $T_g$ . Offline, *worlds* generates trace-driven traffic and labels, runs the same runtime to log gating decisions, and replays WFQ to report detection metrics and queue-tail and collateral outcomes; labels are used only for reporting. Solid arrows: deployed online loop. Dashed arrows: offline evaluation harness.

For contention stealth, let  $C(i)$  be the contention clique containing flow  $i$ . Under baseline WFQ replay *without defensive gating*, let  $d_n$  be the queueing delay (enqueue-to-dequeue time) experienced by packet  $n$  in clique  $C$ . Define the clique mean delay over the horizon as

$$\bar{D}_C = \frac{1}{|\mathcal{P}_C|} \sum_{n \in \mathcal{P}_C} d_n, \quad (6)$$

where  $\mathcal{P}_C$  is the set of packets belonging to flows in clique  $C$  during  $[0, H\Delta t]$ . We write  $\bar{D}_C^{\text{ben}}$  and  $\bar{D}_C^{\text{atk}}$  for the mean delays under benign-only and attack-injected traces, respectively.

Some triples  $(R_i^{\min}, \epsilon, \delta_q)$  are infeasible for a given world and clique load, so feasibility is treated as a first-class outcome. When a requested triple is infeasible, the generator either declares infeasibility under the requested budgets or attempts to restore feasibility by reducing offered load while preserving the throughput floor when possible. If the throughput floor cannot be met jointly with  $(\epsilon, \delta_q)$ , the attempt is declared infeasible. We report feasibility rates for each budget setting.

TABLE II  
OPERATIONAL BUDGETS DEFINING TIMING-CONTROLLED EVASION IN worlds.

Budget	Symbol	Units	Definition
Throughput floor	$R_i^{\min}$	bytes	$\sum_{n \in i, t_n \in [0, H\Delta t]} \ell_n \geq R_i^{\min}$
Timing distortion	$\epsilon$	s	$\frac{1}{ \mathcal{T}_i } \sum_{t \in \mathcal{T}_i} W_1(\bar{P}_{i,t}^{\text{iat}}, \bar{P}_i^{\text{ben,iat}}) \leq \epsilon$
Contention stealth	$\delta_q$	s	$\bar{D}_{C(i)}^{\text{atk}} - \bar{D}_{C(i)}^{\text{ben}} \leq \delta_q$

### E. Defender evaluation under stand-alone thresholding

For flow  $i$  and window  $t$ , the detector outputs a score  $s_{i,t}$  and a binary alarm

$$a_{i,t} = \mathbb{I}\{s_{i,t} \geq \vartheta_i\}, \quad (7)$$

where  $\vartheta_i$  is set by high-quantile burn-in thresholding (Eq. (1)). Let  $\mathcal{A}(R_i^{\min}, \epsilon, \delta_q)$  denote the admissible adversarial policies that satisfy Table II. For a fixed quantile  $q$ , we evaluate robustness through the achieved detection probability under admissible attacks,

$$\min_{P \in \mathcal{A}(R_i^{\min}, \epsilon, \delta_q)} \Pr_{x \sim P} [s(x) \geq \vartheta_i \mid \text{mal}], \quad (8)$$

and we report the achieved benign false-positive rate induced by the same  $\vartheta_i$  on the held-out test segment.

### F. Evasive policy class: projection-based C2

To avoid cherry-picked evasions, we use a fixed, auditable policy class that directly enforces the three budgets. The generator starts from a malicious proposal schedule, then (i) projects timing within each window to satisfy the Wasserstein constraint, (ii) repairs sizes to maintain the throughput floor, and (iii) enforces contention stealth through iterative load reduction with baseline WFQ replay.

### G. Optional protocol side-channel constraints

When DNS or TLS handshake metadata is visible, we optionally impose additional stealth constraints at the same window cadence. These constraints are orthogonal to the timing-control budgets above and are used only in runs where the required fields are uniformly available.

## IV. NOS-GATE DETECTOR: MAPPING IDS TO NOS DYNAMICS

NOS-Gate instantiates the NOS two-state unit as a streaming intrusion detector at a consumer gateway. The two-state dynamics, bounded excitability, recovery coupling, and damping terms are inherited from NOS. The change is the meaning of the exogenous drive: in NOS networking it represents queue and interference forcing, whereas in NOS-Gate it is a metadata-only evidence signal computed per flow per window. This retains the NOS structure while changing what the “input” represents.

Table III provides an auditable correspondence between the NOS symbols and their IDS interpretation, and makes clear what is reused unchanged and what is reinterpreted for detection and action.

**Algorithm 1** Projection-based evasive C2 generator (per flow)

**Require:** Benign IAT reference  $P_i^{\text{ben},\text{iat}}$ , size bounds  $[\ell_{\min}, \ell_{\max}]$ , window size  $\Delta t$ , horizon  $H$ , bytes floor  $R_i^{\min}$ , distortion radius  $\varepsilon$ , delay tolerance  $\delta_q$ , max iters  $I_{\max}$

**Ensure:** Packet times  $\{t_n\}$  and sizes  $\{\ell_n\}$  for flow  $i$  over  $[0, H\Delta t]$ , or infeasibility flag

- 1: **Initialise** a proposal schedule with packet times and sizes satisfying  $\sum_n \ell_n \geq R_i^{\min}$
- 2: **for**  $t = 0$  to  $H - 1$  **do**
- 3:   Extract packets in window  $t$  and compute  $N_{i,t}$
- 4:   **if**  $N_{i,t} \geq 2$  **then**
- 5:     Compute  $\hat{P}_{i,t}^{\text{iat}}$  and  $d_t \leftarrow W_1(\hat{P}_{i,t}^{\text{iat}}, P_i^{\text{ben},\text{iat}})$
- 6:     **if**  $d_t > \varepsilon$  **then**
- 7:       **Project timing in window:** apply an order-preserving time-warp on  $[t\Delta t, (t+1)\Delta t)$   
so the resulting IAT empirical distribution satisfies  
 $W_1 \leq \varepsilon$   
(implementation: quantile mapping on sorted IATs with minimal interpolation)
- 8:       **end if**
- 9:     **end if**
- 10:   **Repair throughput locally:** adjust packet sizes within  $[\ell_{\min}, \ell_{\max}]$  to keep cumulative bytes on track for  $R_i^{\min}$
- 11: **end for**
- 12: Run baseline WFQ replay (no gating) for clique  $C(i)$  to estimate  $\bar{D}_{C(i)}^{\text{atk}}$
- 13: **for**  $\ell = 1$  to  $I_{\max}^{\text{ben}}$  **do**
- 14:   **if**  $\bar{D}_{C(i)}^{\text{atk}} - \bar{D}_{C(i)}^{\text{ben}} \leq \delta_q$  **then**
- 15:     **return** packet times and sizes
- 16:   **end if**
- 17:   **Reduce offered load:** decrease packet emission while attempting to preserve  $\sum_n \ell_n \geq R_i^{\min}$
- 18: Re-apply the per-window projection and size repair steps
- 19: Re-estimate  $\bar{D}_{C(i)}^{\text{atk}}$  by baseline WFQ replay
- 20: **end for**
- 21: **return infeasible** under  $(R_i^{\min}, \varepsilon, \delta_q)$

**A. Design rationale: why a two-state NOS unit helps under timing control**

NOS-Gate targets the gateway loop in Figure 1: flows must be scored online at a fixed cadence, thresholds must be set without labels, and decisions should drive a reversible action with measurable queue impact. Under the threat model, the attacker can time-warp within windows and reshape burst structure subject to a throughput floor and a timing-distortion budget. This often reduces sharp per-window signatures and pushes attacks toward smaller deviations that persist over longer periods.

Stand-alone thresholding makes this harder. Each flow threshold  $\vartheta_i$  is set by a high burn-in quantile (Eq. (1)) and then frozen. A detector that relies on rare, high-amplitude score spikes is easier to suppress because the attacker only needs to keep scores below a tail threshold. A detector that can accumulate modest deviations over time is more likely to cross a high quantile without requiring any single window to

look extreme.

With coupling disabled by default ( $g = 0$ ), NOS-Gate acts as a per-flow streaming mechanism driven by the scalar evidence  $E_{i,t}$  in Eq. (11). Around the benign operating band, the  $v$ -update behaves like a leaky evidence accumulator, while the recovery state  $u$  provides slower negative feedback. The leak terms prevent unbounded accumulation, the bounded nonlinearity reduces sensitivity to rare transients, and the explicit  $-u$  term suppresses repeated triggering after sustained elevation. The event surrogate  $S_{i,t} = \sigma_k(v_{i,t})$  converts this filtered state into a bounded readout that is straightforward to calibrate using a high-quantile rule.

**B. From gateway flows to NOS nodes**

We model each active directed flow  $i$  as a node in a contention structure with nonnegative weights  $W = [w_{ij}]$ . Two flows are neighbours if they compete for the same gateway scheduling domain (uplink WFQ domain or a contention clique). The NOS graph-local input is retained:

$$I_{i,t} = g \sum_{j \in \mathcal{N}(i)} w_{ij} S_{j,t-L_{ij}}, \quad (9)$$

where  $g$  is a global coupling gain,  $L_{ij} \in \mathbb{Z}_{\geq 0}$  is an integer delay in windows, and  $S_{j,t}$  is an event surrogate emitted by flow  $j$  (defined below). In the main results we set  $g = 0$  unless stated otherwise; coupling is evaluated in ablations. NOS-Gate updates all flows synchronously once per window. Since the neighbour surrogate  $S_{j,t}$  is emitted at window  $t$  and coupling is applied when advancing to  $t+1$ , the smallest realised coupling delay is one window. We therefore parameterise an *additional* delay  $\tau_{ij} \in \mathbb{Z}_{\geq 0}$  and define the implemented delay index as

$$L_{ij} = 1 + \tau_{ij}. \quad (10)$$

Thus  $\tau_{ij} = 0$  corresponds to the minimum one-window lag, and the effective physical delay is  $(1 + \tau_{ij})\Delta t$  seconds.

**C. State interpretation for IDS**

NOS-Gate reuses the two NOS states with an IDS interpretation that preserves their mathematical roles:

$$v \mapsto \text{bounded evidence accumulation (suspicion)},$$

$$u \mapsto \text{recovery state (suppression resource).}$$

Operationally,  $v$  behaves like a virtual evidence queue that rises when metadata features deviate from benign patterns and drains under damping. The recovery state  $u$  increases under sustained elevation and pulls  $v$  down via the explicit  $-u$  term, which reduces rapid re-triggering after a burst of alarms. When we include  $u$  in a score readout, we treat it as a persistence indicator correlated with sustained deviation, not as a direct alarm trigger by itself.

**D. Evidence drive as a magnitude input**

For each flow  $i$  and window  $t$ , we compute a normalised feature vector  $\hat{x}_{i,t} \in \mathbb{R}^d$  (Section V) and map it to a scalar evidence drive

$$E_{i,t} = \zeta \|\hat{x}_{i,t}\|_p, \quad (11)$$

where  $p \geq 1$  and  $\zeta > 0$  are hyperparameters. We treat  $E_{i,t}$  as constant over the window  $[t\Delta t, (t+1)\Delta t)$ . Because  $\hat{x}_{i,t}$  is produced by online z-scoring, the norm aggregates multi-feature deviations without labels and avoids learning per-feature weights.

### E. NOS dynamics for IDS (windowed discretisation)

NOS-Gate runs once per window, so we discretise the NOS two-state dynamics with an explicit Euler step of size  $\Delta t$ . Let  $v_{i,t} \approx v_i(t\Delta t)$  and  $u_{i,t} \approx u_i(t\Delta t)$ .

#### Event surrogate (readout used for coupling and scoring).

$$S_{i,t} = \sigma_k(v_{i,t} - \theta) = \frac{1}{1 + \exp(-k(v_{i,t} - \theta))}. \quad (12)$$

**Neighbour drive (optional).** When coupling is enabled, the NOS graph-local term is Eq. (9). We update all flows synchronously once per window. Since  $S_{j,t}$  is produced at window  $t$  and is only available when advancing to  $t+1$ , the minimum realised coupling lag is one window. We therefore parameterise an additional delay  $\tau_{ij} \in \mathbb{Z}_{\geq 0}$  and implement  $L_{ij} = 1 + \tau_{ij}$ , so  $\tau_{ij} = 0$  corresponds to the minimum one-window lag.

**Bounded excitability.** We use the NOS bounded nonlinearity

$$f_{\text{sat}}(v) = \frac{\alpha v^2}{1 + \kappa v^2}, \quad (13)$$

with  $\alpha > 0$  and  $\kappa > 0$ . For numerical safety, the implementation may clip  $v$  to  $[0, v_{\max}]$

#### State update (same NOS core, with IDS-specific drive).

Define the total exogenous drive as the sum of the IDS evidence and (optionally) the neighbour drive:  $A_{i,t} = E_{i,t} + I_{i,t}$  (set  $I_{i,t} = 0$  when coupling is disabled). The per-window updates are

$$v_{i,t+1} = v_{i,t} + \Delta t \left( f_{\text{sat}}(v_{i,t}) + \beta v_{i,t} + \gamma - u_{i,t} + A_{i,t} - \lambda v_{i,t} - \chi(v_{i,t} - v_{\text{rest}}) \right) c + \xi_{i,t} - r S_{i,t}, \quad (14)$$

$$u_{i,t+1} = u_{i,t} + \Delta t \left( ab v_{i,t} - (a + \mu) u_{i,t} \right). \quad (15)$$

Here  $\xi_{i,t}$  is an optional zero-mean noise term (set to 0 unless enabled) and  $v_{\text{rest}}$  is the benign baseline (we use  $v_{\text{rest}} = 0$  unless stated). The optional term  $-rS_{i,t}$  is a continuous reset pathway (set  $r = 0$  when not used). This is the only structural difference from NOS: the “input” is now  $A_{i,t}$ , whose IDS component is  $E_{i,t}$  from Eq. (11).

### F. Score, alarm, and WFQ gating action

NOS-Gate converts state into an anomaly score

$$s_{i,t} = \eta_1 S_{i,t} + \eta_2 u_{i,t}. \quad (16)$$

An alarm is  $a_{i,t} = \mathbb{I}\{s_{i,t} \geq \vartheta_i\}$ , where  $\vartheta_i$  is set per flow by burn-in quantile thresholding (Eq. (1)). We stabilise alerts with the  $K$ -of- $M$  persistence rule (Section II). When actionable, WFQ gating assigns  $\omega_i = \omega_-$  for  $T_g$ ; otherwise  $\omega_i = \omega_0$ .

In the main results we use  $\eta_2 = 0$ , so the operational score is driven by  $S_{i,t}$ . We use  $\eta_2 > 0$  only in ablations, where  $u_{i,t}$  acts as a slow-burn persistence cue. The run manifest records  $(\eta_1, \eta_2)$ .

### G. Fixed points and stability

For constant drives (that is,  $E_{i,t} \equiv E_i^*$  and  $I_{i,t} \equiv I_i^*$ ), with  $\xi_{i,t} = 0$  and  $r = 0$ , a steady state  $(v_i^*, u_i^*)$  of the underlying NOS core satisfies

$$0 = f_{\text{sat}}(v_i^*) + \beta v_i^* + \gamma - u_i^* + E_i^* + I_i^* - \lambda v_i^* - \chi(v_i^* - v_{\text{rest}}), \quad (17)$$

together with  $ab v_i^* = (a + \mu) u_i^*$  from Eq. (15). (If the optional reset  $r > 0$  is enabled, it adds an additional negative feedback

TABLE III  
AUDITABLE MAPPING FROM NOS (MAIN MODEL) TO NOS-GATE (IDS INSTANTIATION).

Symbol	NOS meaning	NOS-Gate (IDS) meaning
$v_i$	Normalised congestion proxy	Bounded evidence accumulation, optionally clipped to $[0, v_{\max}]$
$u_i$	Recovery / slowdown resource	Suppression state damping
$f_{\text{sat}}(v)$	Bounded excitability (finite buffers)	Bounded evidence growth under deviation
$\beta v_i + \gamma$	Residual slope and offset	Bias and linear drift correction
$-u_i$	Post-burst recovery drag	Refractory suppression after alarms
$-\lambda v_i$	Service-like drainage	Evidence decay toward baseline
$-\chi(v_i - v_{\text{rest}})$	Small-signal damping	Stabilisation around benign baseline
$I_i(t)$	Graph-local coupling	Contention-driven neighbour propagation (ablation)
$S_i(t)$	Presynaptic event train	Event surrogate $S_{i,t} = \sigma_k(v_{i,t} - \theta)$
$(a, b, \mu)$	Recovery sensitivity and decay	Suppression build-up and persistence
Exogenous drive	Telemetry forcing	Total drive $A_{i,t} = E_{i,t} + I_{i,t}$ with $E_{i,t} = \zeta \ \hat{x}_{i,t}\ _p$
Reset pathway	Differentiable reset option	Optional continuous reset $-rS_{i,t}$
Operational action	Operator control	WFQ gating: alarms reduce weight $\omega_i$

term proportional to  $S_i^* = \sigma_k(v_i^* - \theta)$  in the discrete-time update in Eq. (14).)

For conservative calibration checks, we isolate the coupling gain. Since  $\max_x \sigma'_k(x) = k/4$ , the linearised coupling path in the  $v$ -update is bounded by  $\Delta t g \rho(W) k/4$ . In experiments we choose  $(g, k)$ ,  $\Delta t$ , and the world-specific  $\rho(W)$  band so that this bound remains below the local damping and recovery margin induced by  $(\lambda, \chi)$  and  $(a, b, \mu)$ , and the local slope of  $f_{\text{sat}}$  around the operating band. The IDS evidence  $E_{i,t}$  enters only as exogenous forcing.

## V. METHODS

NOS-Gate operates on per-flow packet metadata at a fixed cadence. We treat each directed five-tuple flow as a stream and summarise its packets in non-overlapping windows of length  $\Delta t = 250$  ms. Each window yields one feature vector  $x_{i,t}$  for flow  $i$  at window index  $t$ . In synthetic worlds, flow keys and (when needed) device identifiers are known by construction. In the optional corpus mode, we extract the same directed five-tuple flows from PCAP or flow logs. Device identity is not required for scoring, but when a stable identifier exists (for example, a MAC address or a DHCP lease), we maintain separate normalisation statistics per device.

### A. Causal windowing and online normalisation

All feature computation is causal. Features for window  $t$  use only packets with timestamps in  $[t\Delta t, (t+1)\Delta t)$ , and any running statistics depend only on earlier windows. After computing  $x_{i,t}$ , we normalise online to reduce drift and make thresholds comparable across flows.

Let  $d(i)$  be the device identifier for flow  $i$  when available (otherwise a single global bucket). For each feature index  $k$  and device bucket  $d$ , we maintain exponential running mean and variance,

$$m_{t+1}^{(d,k)} = (1 - \lambda_m)m_t^{(d,k)} + \lambda_m x_t^{(d,k)}, \quad (18)$$

$$q_{t+1}^{(d,k)} = (1 - \lambda_v)q_t^{(d,k)} + \lambda_v (x_t^{(d,k)} - m_t^{(d,k)})^2, \quad (19)$$

and emit a z-score

$$\hat{x}_{t+1}^{(d,k)} = \frac{x_t^{(d,k)} - m_t^{(d,k)}}{\sqrt{q_t^{(d,k)} + \epsilon}}. \quad (20)$$

Operationally, we compute  $\hat{x}_{i,t}$  using  $(m_t, q_t)$ , score window  $t$ , and then update  $(m_{t+1}, q_{t+1})$  using  $x_{i,t}$ . We use separate rates  $\lambda_m$  and  $\lambda_v$  so that the variance adapts more cautiously than the mean under bursty traffic. If a window has no packets, rate features are set to zero and IAT summaries are marked as missing (the evidence drive in Eq. (11) remains defined through other features). We clip z-scores to a fixed magnitude (default 8) to prevent a single spike from dominating. Thresholds are fixed after burn-in. To limit post burn-in drift, online mean and variance updates use a small adaptation rate and are clipped to prevent abrupt shifts. We also evaluated freezing normalisation after burn-in and observed similar qualitative trends, at the cost of slightly higher false positives; we leave systematic adversarial drift handling to future work.

### B. Feature contract

The feature stream is deliberately small and restricted to fields visible at the gateway: headers, timestamps, and sizes, plus DNS and TLS handshake metadata when present. From timing and burstiness we include packet rate, simple inter-arrival summaries (mean and coefficient of variation when at least two packets exist), and a low-frequency pacing indicator computed from counts in  $B$  fixed micro-bins within the window. From contention we include (i) clique-level rate share and (ii) an interference index derived from the contention weights  $W$  used by the *worlds* generator.

When DNS or TLS handshake metadata is available, we add a small set of additional fields (for example, domain churn, TTL variance, and coarse certificate attributes). When these fields are absent, we drop them rather than impute values, and we report results under a fixed feature contract per run. The run manifest records the feature contract and discrete settings (including  $B$  and the z-score clip magnitude).

### C. End-to-end loop and replay-based impact evaluation

The online pipeline is identical in synthetic and corpus modes. The *worlds* generator emits packet traces with flow keys, timestamps, and sizes, together with contention structure and evasion budgets (Table II). We window packets to produce  $x_{i,t}$ , normalise online to obtain  $\hat{x}_{i,t}$ , and run NOS-Gate as a per-flow streaming update (Section IV).

All detectors, including baselines, follow the same stand-alone operating protocol. An assumed-benign burn-in segment is used for training (where applicable) and for collecting burn-in scores. Each flow threshold is then set as a high quantile of burn-in scores (Eq. (1)) and frozen for test. Labels are used only for reporting on held-out time.

Queue impact is evaluated by packet-level WFQ replay in two conditions: (i) baseline replay without gating and (ii) replay with gating driven by each method's actionable flags  $z_{i,t}$ . Replay logs are produced in microseconds; we report queue metrics in milliseconds for readability. Efficiency is reported as microseconds per (flow, window) record, since gateway cost scales primarily with active flows and the window cadence.

## VI. RESULTS

We report results on reproducible worlds containing malicious episodes under the timing-controlled threat model. All methods operate in a stand-alone, label-free mode: per-flow thresholds are set from the burn-in segment using the same high-quantile rule and then frozen for test (Eq. (1)). We report two alert budgets,  $FPR = 1\%$  and  $FPR = 0.1\%$ , and we always show the *achieved* benign false-alarm rate on the held-out test segment under that protocol.

### A. Incident detection under timing-controlled evasion

Figure 2 summarises incident recall and time-to-detect (TTD) at  $FPR = 0.1\%$ . This operating point is intentionally strict. Because  $\vartheta_i$  is a high burn-in quantile and is then frozen, a detector must exceed a tail threshold on each flow. Under timing-controlled evasion (Table II), the attacker can often reduce sharp per-window anomalies by spreading activity across windows while still meeting the throughput floor. This makes methods that depend on occasional high-amplitude windows easier to suppress below  $\vartheta_i$ , while methods that accumulate modest deviation energy across time are more likely to trigger without relying on a single extreme window.

At  $FPR = 0.1\%$ , NOS-Gate misses 1 of 21 incidents (incident recall 0.952). The strongest baseline in these runs, TinyGRU, misses 3 incidents (recall 0.857). The remaining baselines miss 5 incidents (recall 0.762).

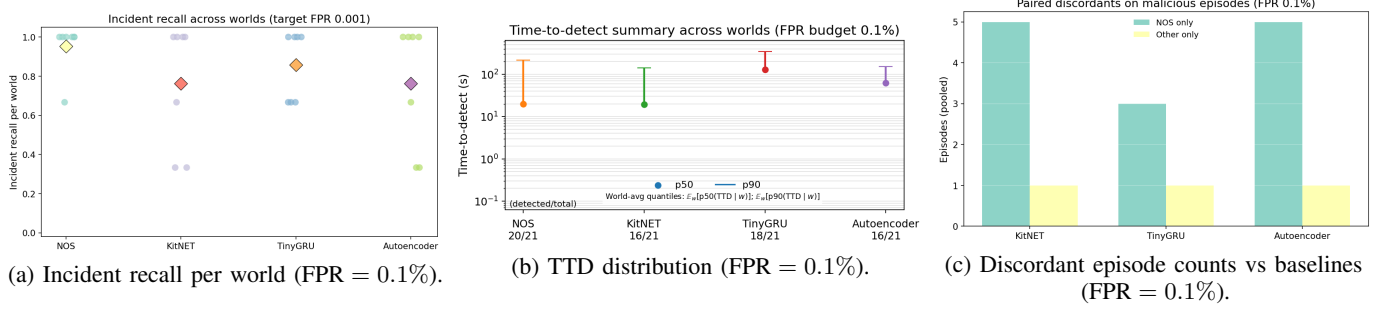
Figure 2(a) shows per-world recall and indicates that the gain is not driven by a single outlier world. Figure 2(b) shows the TTD distribution over detected incidents. Several baselines can trigger quickly when they trigger, but under the strict budget they fail to trigger on more episodes. NOS-Gate trades some latency on the hardest cases for fewer missed incidents, which is the relevant trade-off when false alarms must remain rare.

Figure 2(c) provides episode-level discordant counts pooled across the same 21 episodes. NOS-Gate detects more episodes that each baseline misses than vice versa (KitNET: 5 vs 1; TinyGRU: 3 vs 1; autoencoder: 5 vs 1). The sample is modest, so we treat this as supporting evidence rather than a standalone statistical claim, but the direction is consistent across baselines.

### B. Queue impact of WFQ gating

Detection is evaluated here through its control effect. We therefore assess WFQ gating using packet-level replay, driven by each method's actionable flags under the strict operating point ( $FPR = 0.1\%$ ). Queue logs are produced in microseconds and reported in milliseconds.

Figure 3 reports tail queueing delay and tail collateral delay under gating (p99.9). NOS-Gate is the only method

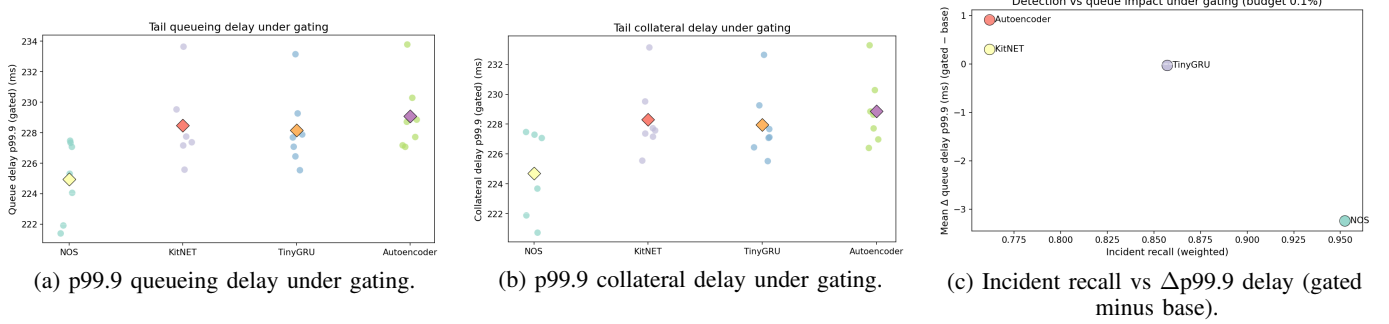


(a) Incident recall per world (FPR = 0.1%).

(b) TTD distribution (FPR = 0.1%).

(c) Discordant episode counts vs baselines (FPR = 0.1%).

Fig. 2. Detection under the strict false-alarm budget. Panels (a) and (b) show per-world behaviour and latency dispersion, not only pooled totals. Panel (c) summarises episode-level discordants (NOS-Gate only vs baseline), pooled across worlds.

Fig. 3. Action-level evaluation under the strict operating point (FPR = 0.1%). NOS-Gate is the only method that improves both queue-tail delay and collateral tail delay while maintaining the highest incident recall under the same label-free calibration protocol. Delays are reported in ms (raw logs are in  $\mu$ s).

that improves both metrics consistently across the 7 worlds. Relative to baseline replay without gating, NOS-driven gating reduces p99.9 queueing delay by about 3.24 ms on average across worlds and reduces p99.9 collateral delay by about 3.16 ms. In contrast, gating driven by KitNET and the autoencoder increases mean p99.9 queueing delay in these runs (about +0.30 ms and +0.91 ms, respectively), which is consistent with less targeted gating under the same strict alert budget.

Figure 3(c) summarises the central deployment question: under a strict alert cap, does the detector sit in the favourable region of higher incident recall and lower tail delay. Under the shared stand-alone protocol, NOS-Gate occupies that region in these worlds.

### C. Efficiency on CPU

Table IV reports scoring cost in microseconds per window-row. NOS-Gate remains lightweight (mean  $\approx$  2.09  $\mu$ s/row), comparable to the compact autoencoder and substantially faster than KitNET and TinyGRU in these runs. This matters because gateway cost scales with active flows and window cadence. A method that is expensive per window is harder to sustain without adding latency.

### D. Summary

Across these runs, NOS-Gate is the only method that meets the three constraints that define the gateway setting at once: (i) under a strict false-alarm budget it misses fewer incidents, (ii) its actionable flags drive a reversible WFQ action that reduces both queue-tail delay and collateral tail delay in replay, and (iii) it achieves this with a small, stable per-window compute cost.

TABLE IV  
SCORING COST ON CPU (MICROSECONDS PER WINDOW-ROW).

Method	Mean ( $\mu$ s/row)	p90 ( $\mu$ s/row)	Max ( $\mu$ s/row)
NOS-Gate	2.09	2.97	2.99
Autoencoder	2.03	2.78	2.80
KitNET	11.68	16.72	16.80
TinyGRU	31.10	46.57	49.24

Under looser thresholds, baselines can appear closer. The strict stand-alone calibration exposes the failure mode that matters operationally: missed incidents and action-triggered latency when alerts must be rare.

## VII. CONCLUSION

Consumer gateways in the networks sit at the point where encrypted services meet heterogeneous IoT devices, but encryption leaves timing, size, and burst structure visible. Those side channels support metadata-based IDS, yet they also create a practical evasion surface: an adaptive adversary can reshape timing while still meeting an attack objective. This paper addressed a deployment-centred question: under a strict false-alarm cap and without labels, can a gateway detect quickly enough to act, using only metadata, and can that action reduce user-visible queue harm rather than add to it? We introduced *NOS-Gate*, a streaming IDS that instantiates a lightweight two-state unit derived from Network-Optimised Spiking (NOS) dynamics per flow. The model is structurally faithful to NOS and changes only the interpretation of the exogenous drive, which becomes a scalar evidence signal derived from online normalised metadata features. The resulting

state update provides controlled leak, bounded growth, and recovery-driven suppression, producing a stable score that is calibrated stand-alone by burn-in quantile thresholding and stabilised by a  $K$ -of- $M$  persistence rule. Crucially, NOS-Gate connects detection to an auditable mitigation path by temporarily reducing WFQ weights for persistently suspicious flows. To evaluate this action loop under timing-controlled evasion, we introduced an executable *worlds* benchmark with explicit attacker budgets and packet-level WFQ replay. Under the strict operating point (0.1% achieved benign false-positive rate), NOS-Gate achieved the highest incident recall among the tested label-free baselines while also improving tail queue outcomes under gating, including reduced p99.9 queueing delay and reduced collateral tail delay. Its per-window scoring cost remained small and stable on CPU, which matches gateway scaling constraints. Finally, we do not claim payload-level coverage or that synthetic worlds capture every real deployment. Instead, we offer a falsifiable protocol, artefacts, and budgets that make both evasion and queue impact measurable. Future work should expand the benchmark with additional device processes, and explore how learned feature representations can be introduced without breaking the stand-alone calibration and action-audit requirements.

## REFERENCES

- [1] M. Bilal, "Network-optimised spiking neural network for event-driven networking," *arXiv preprint arXiv:2509.23516*, 2025. [Online]. Available: <https://arxiv.org/abs/2509.23516>
- [2] M. Conti, L. V. Mancini, R. Spolaor, and N. V. Verde, "Analyzing android encrypted network traffic to identify user actions," *IEEE Transactions on Information Forensics and Security*, vol. 11, no. 1, pp. 114–125, 2016.
- [3] A. Panchenko, F. Lanze, J. Pennekamp, T. Engel, A. Zinnen, M. Henze, and K. Wehrle, "Website fingerprinting at internet scale," in *Network and Distributed System Security Symposium*, 2016. [Online]. Available: <https://api.semanticscholar.org/CorpusID:15302617>
- [4] A. Sivanathan, H. H. Gharakheili, F. Loi, A. Radford, C. Wijenayake, A. Vishwanath, and V. Sivaraman, "Classifying iot devices in smart environments using network traffic characteristics," *IEEE Transactions on Mobile Computing*, vol. 18, no. 8, pp. 1745–1759, 2019.
- [5] M. Miettinen, S. Marchal, I. Hafeez, N. Asokan, A.-R. Sadeghi, and S. Tarkoma, "Iot sentinel: Automated device-type identification for security enforcement in iot," in *2017 IEEE 37th International Conference on Distributed Computing Systems (ICDCS)*, 2017, pp. 2177–2184.
- [6] I. Hafeez, M. Antikainen, A. Y. Ding, and S. Tarkoma, "Iot-keeper: Detecting malicious iot network activity using online traffic analysis at the edge," *IEEE Transactions on Network and Service Management*, vol. 17, no. 1, pp. 45–59, 2020.
- [7] T. D. Nguyen, S. Marchal, M. Miettinen, H. Fereidooni, N. Asokan, and A.-R. Sadeghi, "Diot: A federated self-learning anomaly detection system for iot," in *2019 IEEE 39th International Conference on Distributed Computing Systems (ICDCS)*, 2019, pp. 756–767.
- [8] V. Chandola, A. Banerjee, and V. Kumar, "Anomaly detection: A survey," vol. 41, no. 3, 2009.
- [9] Y. Mirsky, T. Doitshman, Y. Elovici, and A. Shabtai, "Kitsune: An ensemble of autoencoders for online network intrusion detection," in *Network and Distributed System Security Symposium (NDSS)*, 2018.
- [10] C. V. Wright, S. E. Coull, and F. Monroe, "Traffic morphing: An efficient defense against statistical traffic analysis," in *Network and Distributed System Security Symposium (NDSS)*, 2009.
- [11] X. Cai, R. Nithyanand, T. Wang, R. Johnson, and I. Goldberg, "A systematic approach to developing and evaluating website fingerprinting defenses," New York, NY, USA: Association for Computing Machinery, 2014.
- [12] M. Bilal and X. Xu, "Network-optimised spiking neural network (nos) scheduling for 6g o-ran: Spectral margin and delay-tail control," *arXiv preprint arXiv:2510.11291*, 2025. [Online]. Available: <https://arxiv.org/abs/2510.11291>
- [13] A. Tavvaei, M. Ghodrati, S. R. Kheradpisheh, T. Masquelier, and A. Maida, "Deep learning in spiking neural networks," *Neural Networks*, vol. 111, pp. 47–63, 2019.
- [14] D. Marković, A. Mizrahi, D. Querlioz, and J. Grollier, "Physics for neuromorphic computing," *Nature Reviews Physics*, 2020.
- [15] A. Demers, S. Keshav, and S. Shenker, "Analysis and simulation of a fair queueing algorithm," *SIGCOMM Comput. Commun. Rev.*, vol. 19, no. 4, p. 1–12, 1989. [Online]. Available: <https://doi.org/10.1145/75247.75248>
- [16] A. Parekh and R. Gallager, "A generalized processor sharing approach to flow control in integrated services networks: the single-node case," *IEEE/ACM Transactions on Networking*, vol. 1, no. 3, pp. 344–357, 1993.
- [17] A. K. Parekh and R. G. Gallager, "A generalized processor sharing approach to flow control in integrated services networks: The multiple-node case," *IEEE/ACM Transactions on Networking*, vol. 2, no. 2, 1994.
- [18] K. Nichols and V. Jacobson, "Controlling queue delay," *Queue*, vol. 10, no. 5, 2012.
- [19] C. Fu, Q. Li, and K. Xu, "Detecting unknown encrypted malicious traffic in real time via flow interaction graph analysis," in *Network and Distributed System Security Symposium (NDSS)*, 2023.
- [20] Y. Qing, Q. Yin, X. Deng, Y. Chen, Z. Liu, K. Sun, K. Xu, J. Zhang, and Q. Li, "Low-quality training data only? A robust framework for detecting encrypted malicious network traffic," in *Network and Distributed System Security Symposium (NDSS)*, 2024.
- [21] L. Gao, C. Fu, X. Deng, K. Xu, and Q. Li, "Wedjat: Detecting sophisticated evasion attacks via real-time causal analysis," in *Proceedings of the 31st ACM SIGKDD Conference on Knowledge Discovery and Data Mining V.1*, ser. KDD '25. New York, NY, USA: Association for Computing Machinery, 2025, p. 342–353. [Online]. Available: <https://doi.org/10.1145/3690624.3709218>
- [22] S. Sattar, S. Khan, M. I. Khan, A. Akhmediyarova, O. Mamyrbayev, D. Kassymova, D. Oralbekova, and J. Alimkulova, "Anomaly detection in encrypted network traffic using self-supervised learning," *Scientific Reports*, vol. 15, p. 26585, 2025. [Online]. Available: <https://www.nature.com/articles/s41598-025-08568-0>
- [23] Y. Meidan, M. Bohadana, Y. Mathov, Y. Mirsky, A. Shabtai, D. Breitenbacher, and Y. Elovici, "N-baito—network-based detection of iot botnet attacks using deep autoencoders," *IEEE Pervasive Computing*, vol. 17, no. 3, pp. 12–22, 2018.
- [24] S. Sicari, A. Rizzardi, L. Grieco, and A. Coen-Porisini, "Security, privacy and trust in internet of things: The road ahead," *Computer Networks*, vol. 76, pp. 146–164, 2015. [Online]. Available: <https://www.sciencedirect.com/science/article/pii/S1389128614003971>
- [25] H. Tahaei, F. Afifi, A. Asemi, F. Zaki, and N. B. Anuar, "The rise of traffic classification in iot networks: A survey," *Journal of Network and Computer Applications*, vol. 154, p. 102538, 2020.
- [26] A. L. Buczak and E. Guven, "A survey of data mining and machine learning methods for cyber security intrusion detection," *IEEE Communications Surveys & Tutorials*, vol. 18, no. 2, pp. 1153–1176, 2016.